THE GRAVITY-PROBE-B RELATIVITY GYROSCOPE EXPERIMENT: DEVELOPMENT OF THE PROTOTYPE FLIGHT INSTRUMENT

J. P. Turneaure,* C. W. F. Everitt,* B. W. Parkinson,* D. Bardas,*
J. V. Breakwell,** S. Buchman,* W. S. Cheung,*
D. E. Davidson,*** D. B. DeBra,** W. M. Fairbank,* S. Feteih,*
D. Gill,* R. Hacker,** G. M. Keiser,* J. M. Lockhart,†
B. Muhlfelder,* R. T. Parmley,‡ Xinhua Qin,* M. A. Taber,*
R. A. Van Patten,** Y. M. Xiao* and P. Zhou§

*W. W. Hansen Laboratories of Physics; **Department of Aeronautics and Astronautics, Stanford University, Stanford, CA 94305, U.S.A.
***Optical Instrument Design, Mathews, VA 23109, U.S.A.
†Physics Department, San Francisco State University, San Francisco, CA 94117, U.S.A.
‡Research and Development Division, Lockheed Missiles and Space Company, Inc., 3251 Hanover Street, Palo Alto, CA 94304, U.S.A.
§Institute of Physics, Chinese Academy of Sciences, Beijing, China

ABSTRACT

The Gravity-Probe-B Relativity Gyroscope Experiment (GP-B) will measure the geodetic and frame-dragging precession rates of gyroscopes in a 650 km high polar orbit about the earth. The goal is to measure these two effects, which are predicted by Einstein's General Theory of Relativity, to 0.01% (geodetic) and 1% (frame-dragging). This paper presents the development progress for full-size prototype flight hardware including the gyroscopes, gyro readout and magnetic shielding system, and an integrated ground test instrument. Results presented include gyro rotor mass-unbalance values (15-86 nm) due to the thickness variations of the thin niobium coating on the rotor, interior sphericities (163-275 nm peak-to-valley) of fused-quartz gyro housings produced by tumble lapping, gyro precession rates (gyroscopes at 5 K) which imply low mass-unbalance components parallel to the gyro axis (23-62 nm), and demonstration of a magnetic shielding factor of 2x10^10 for the gyro readout system with one shielding component missing (the gyro rotor). All of these results are at or near flight requirements for the GP-B Science Mission, which is expected to be launched in 1995.

INTRODUCTION

The Gravity-Probe-B Relativity Gyroscope Experiment (GP-B) is designed to measure two effects predicted by Einstein's General Theory of Relativity: the geodetic and frame-dragging precession rates of gyroscopes /1/. When a gyroscope is in a 650 km high polar orbit about the earth, these two effects are calculated to be 6.6 arc-sec/yr (geodetic) and 0.042 arc-sec/yr (frame-dragging). Precise experimental knowledge of these two effects may aid in the development of gravitational theory and its possible unification with the other forces of nature, and in the interpretation of astrophysical observations /2/. Our goal is to measure the geodetic effect to better than 0.01% and the frame-dragging effect to better than 1%. The experimental concepts and configuration to reach this goal have been discussed elsewhere /3/.

There are three general classes of error that must be considered in the measurement of the two effects: (1) disturbances to the gyro precession rate from Newtonian torques, (2) noise in the experiment readout chain, and (3) uncertainty in the known value of the proper motion of the guide star Rigel. The uncertainty in the proper motion of Rigel comes from limitations in astrometric data rather than the GP-B experiment, and it is currently estimated to be within 0.9×10^{-3} arc-sec/yr in declination and 1.7×10^{-3} arc-sec/yr in right ascension /4/. We are investigating the possibility of reducing the uncertainty in the proper motion by performing an experiment with the European Space Agency's HIPPARCOS astrometric satellite in time for the GP-B data reduction /5/. Of course, any improved knowledge of proper motion gained after the initial GP-B data reduction can also be used; e.g., greatly improved proper motion measurements with uncertainties of $< 1 \times 10^{-6}$ arc-sec/yr using the proposed space-based optical astrometric interferometer POINTS /6/. The first two classes of error are from the GP-B experiment itself. To meet the goal of measuring the two effects to better than 0.01% (geodetic) and 1% (frame-dragging), the error for the first two classes can be allocated as follows assuming they can be combined on a root square sum basis: for the experiment readout chain, 0.59×10^{-3} arc-sec/yr in declination and 0.30×10^{-3} arc-sec/yr in right ascension; and for disturbance torques, 0.30×10^{-3} arc-sec/yr in any direction.

The GP-B effort is currently focused on developing instrument hardware that meets the experiment goals for error in the geodetic and frame-dragging effects and that is full size and prototypical of flight design concepts. This paper presents the progress on such hardware which includes the gyroscope, gyro readout and magnetic shielding system, and a full-size ground test instrument.
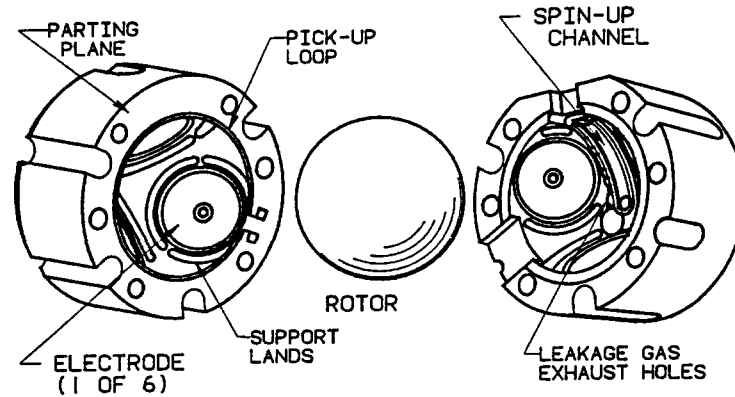

Fig. 1. Exploded view of the gyro rotor and housing.

GYRO MANUFACTURE

Figure 1 is an exploded view of the flight development gyro rotor and its housing. The gyro rotor is a 38 mm diameter sphere of homogeneous fused quartz with a uniform layer of niobium coated on its surface. The rotor is assembled in a housing composed of two halves also made of fused quartz. Each of the halves has three electrodes for electrostatic suspension of the gyro rotor and raised support lands around each electrode to prevent electrical contact between the rotor (when not suspended) and any electrode. In addition, the readout half has a thin-film niobium readout loop located on the parting plane between the halves, and the spinup half has a spinup channel with an inlet and outlet for the helium gas, raised spinup lands to reduce leakage of gas into the gyro during spinup, and an auxiliary channel for differential pumping of the leakage gas through the exhaust holes.

TABLE 1   Principal Manufacturing Requirements for a 0.3×10^{-3} arc-sec/yr Gyroscope

Manufacturing Characteristic	Requirement	Achieved
Rotor Density Homogeneity	$< 2 \times 10^{-6}$ $\Delta\rho/\rho$ across rotor	$< 1.6 \times 10^{-6}$ $\Delta\rho/\rho$
Rotor Sphericity	< 20 nm peak-to-valley	17 nm p-v
Rotor Coating Thickness Uniformity	< 7.5 nm mass unbalance	15 nm
Housing Electrode Substrate Sphericity	< 250 nm peak-to-valley	163 nm p-v
Housing Electrode Coating Uniformity	< 250 nm peak-to-valley	1400 nm p-v

Stringent manufacturing requirements for the gyro rotor and housing are needed to keep the precession rate due to Newtonian disturbance torques below the 0.3×10^{-3} arc-sec/yr allocation given in the introduction. A reanalysis of the Newtonian disturbance torques, which includes the effects of averaging due to (1) gyro spin and polhode motion, (2) spacecraft roll, and (3) orbital and annual motion of the spacecraft, has been initiated by two of the authors (C.W.F. Everitt and G.M. Keiser). The preliminary conclusions indicate that the manufacturing requirements listed in Table 1 should yield a gyroscope meeting the 0.3×10^{-3} arc-sec/yr allocation. This conclusion assumes a gyro spin speed of 170 Hz, a 3×10^{-11} g average acceleration on the gyro transverse to its spin axis, a 2×10^{-7} g electrostatic suspension preload, and a gap between the rotor and the electrode of 25 μm. The assumption of a 3×10^{-11} g average transverse acceleration during flight should be conservative; although the transverse acceleration at the gyroscopes in the frame of the spacecraft-fixed axes is estimated to be 1×10^{-10} g, the roll of the spacecraft would be expected to average this bias to $< 1 \times 10^{-11}$ g in the inertial frame. The first and third requirements given in Table 1 are due to the mass-unbalance disturbance torque (where the mass unbalance is measured by the difference between the rotor center of support and center of mass), and the other requirements are due to disturbance torques coming from the suspension electrode voltages. The values achieved for each requirement are shown in Table 1 and are discussed in the sections below.

Gyro Rotors

Homogeneity. Homosil fused-quartz cubes, about 50 mm on a side, have been supplied by Heraeus-Amersil. The density variation across those cubes has been estimated from Twyman-Green interferograms to be no greater than $1.2-1.6 \times 10^{-6}$ ($\Delta\rho/\rho$) which is below the requirement in Table 1. This estimated homogeneity is limited by the experimental error in the Twyman-Green instrument. Since it is desirable to measure the density variation with greater precision (< 20% of the requirement), M. Player and G. Edgar of the University of Aberdeen, Scotland, are developing an instrument utilizing a laser interferometer (based on earlier work /7/) which should have a measurement error of 5×10^{-8} ($\Delta\rho/\rho$) across the cube /8/.

Sphericity. Fused quartz with the required homogeneity is ground into a rough sphere and then lapped and polished to its final diameter. The final polishing process is the critical step to achieve the required sphericity. The lapping and polishing machines were developed by W. Angele /9/, and a set of machines which were designed and built at the NASA Marshall Space Flight Center are now at Stanford. They are producing spherical rotors on a regular basis. The sphericity is measured with a Talyrond 73 (Rank-Taylor-Hobson) roundness measuring instrument capable of making roundness measurements with an accuracy of 5 nm peak-to-valley /10/. The rotor sphericity error is estimated by measuring the peak-to-valley roundness error for three mutually perpendicular great circles about the rotor. The largest of those errors is taken as an estimate of sphericity error. Of the last 11 rotors polished, 2 out of 11 meet the 20 nm peak-to-valley sphericity error requirement, and 7 out of 11 have sphericity errors of 30 nm peak-to-valley or less. The lowest sphericity error is 17 nm peak-to-valley.

Niobium coating. The fused-quartz rotor is coated with niobium to allow a superconducting London-moment gyro readout and to act as an electrode for electrostatic suspension. The rotor is coated by sputtering niobium downwards to cover somewhat over half the rotor which is held stationary. To yield a uniform coating, the rotor is moved to 32 orientations corresponding to the faces and vertices of a regular icosahedron with an equal amount of niobium deposited for each orientation. This technique was initially conceived and implemented by J.A. Lipa and F.J. van Kann /11/, and then more fully developed by P. Peters /12/.

Rotors are routinely coated at Stanford using this technique. The coating thickness and its uniformity are measured with a β-backscattering thickness measuring instrument at 26 unique locations on the rotor. For the last 6 rotors coated at Stanford, the niobium thickness ranged from 2.5 to 2.7 μm, and the mass-unbalance values, estimated from the thickness data, ranged from 15 to 86 nm. The lowest of these is twice the 7.5 nm requirement given in Table 1. We expect to meet the mass-unbalance requirement by reducing the thickness of the coating (the mass unbalance should approximately scale linearly with thickness) and by improving the coating process and thickness measurement technique.

Gyro Housings

Machining. The matched housing halves are fabricated from fused-quartz blanks into their final shape by ultrasonic machining, diamond grinding, lapping, and polishing. The most demanding requirement for the fabrication is to provide a spherical surface to act as the substrate for the electrodes. As listed in Table 1, this surface is required to be spherical within 250 nm peak-to-valley. To achieve this requirement, approximate hemispheres are formed in the two halves by ultrasonic machining and hand lapping, the halves are precisely joined with tapered fused-quartz pins, and the assembled pair is tumble lapped. Tumble lapping is a process in which a weighted lapping element and slurry of grinding compound and water are located in the spherical cavity formed by the assembled housing, then the housing is randomly rotated about the lapping element.

A tumble-lap machine has been built and tested. This machine has been used to produce the interior spherical surface in several housings. The sphericity error is estimated by measuring the peak-to-valley roundness error of 12 great half-circles for each of the housing halves with a Talyrond 73. The largest of those roundness errors for a housing set is taken as an estimate of the sphericity error. For the four housings that have been tumble lapped and fully measured, the sphericity errors are 163, 250, 238, and 275 nm peak-to-valley: the first three meet the 250 nm sphericity requirement, while the error in the fourth is only 10% above the requirement.

Coating. Four of the housing features are produced by sputter deposition. These include the six suspension electrodes, the support lands around the electrodes, the spinup land, and the gyro readout loop. The first three coatings are all thin copper films with a titanium bonding layer. The electrodes are about 3.5 μm thick and the lands are 13 μm thick. The readout loop is produced by depositing a 400 nm thick niobium layer overcoated with a 20 nm gold layer to assist in bonding wires and then by patterning the loop using either photolithographic or laser milling techniques. All of these coatings have successfully undergone multiple thermal cycles between room temperature and 4 K. Figure 2 is a photograph of a flight development quartz housing with electrode and land coatings.

The six electrodes must be uniformly coated to meet the 250 nm peak-to-valley requirement in Table 1. The electrodes for the first two housings have been coated with uniformities of 1.4 and 1.5 μm peak-to-valley which are several times the requirement. This lack of uniformity comes from the geometries of the housing and the coating mask. A change in the mask geometry which allows the sputter target, mask, and electrode surface to all be symmetric about the same axis should easily yield the required electrode uniformity.
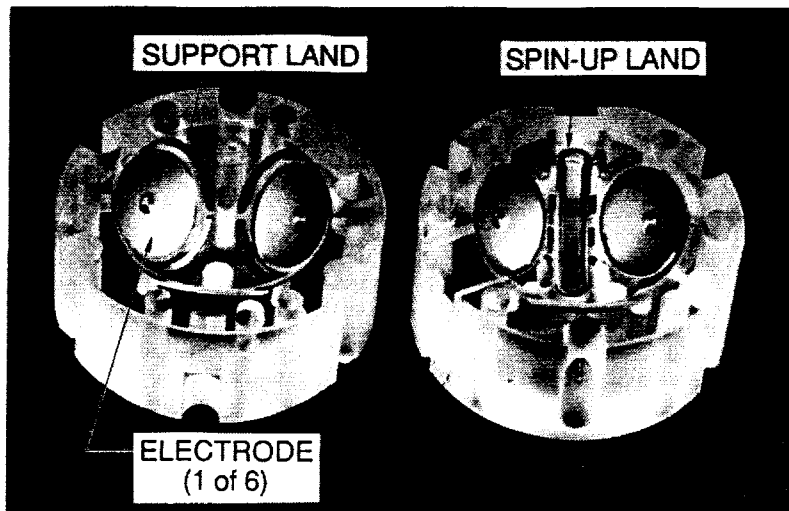

Fig. 2. Photograph of the flight development fused-quartz housing with 3.5 μm thick copper electrodes and 13 μm thick copper support and spinup lands.

GYRO TESTING

Low-Temperature Gyro Testing

Gyroscopes are tested at low temperature in a system called the gimballed gyro test facility. The gyroscope is located in an ultrahigh vacuum, low-temperature probe which is inserted into the well of a liquid helium dewar so the gyroscope can be maintained at 5 K. The mounting and orientation of the gyroscope and the dewar are such that both their axes are aligned parallel to the earth's axis. The gyroscope is suspended and spun up with helium gas. After spinup, the pressure at the gyroscope can be reduced below 10^{-10} torr by increasing the temperature of the gyroscope and its low-temperature environment to 7 K for a few hours and then returning the temperature to its normal operating value (low-temperature, ultrahigh vacuum bakeout). The gyro spin speed, precession, and polhode motion are read out with three orthogonal superconducting loops coupled to superconducting quantum interference devices which measure the motion of magnetic flux trapped in the superconducting niobium rotor coating.

Gyro precession rate. The precession rates for three gyro assemblies have been measured at low temperature in the gimballed gyro test facility. The precession of one gyroscope (Homosil rotor 87-4H and a flight development quartz housing) spinning at about 1.5 Hz is illustrated in Figure 3. (The slow spin speed is used to magnify the effect of the mass-unbalance torque.) Unit gyro spin vector data (derived from the trapped flux measurements) are shown as circles at typical intervals of 90 s. The spin vector starts in a direction approximately aligned with the earth's axis and pointing south, and it then precesses in a counterclockwise direction about the vertical. The center of the precession pattern in the horizontal plane is shifted slightly northward which corresponds to the offset direction expected from the rotation of the laboratory coordinate frame with the earth. Some of the detailed structure seen in Figure 3 appears to be correlated with the location of the suspension electrodes indicating the possible influence of small electrostatic suspension torques.

Table 2 is a summary of the precession rate data for the three gyro assemblies. For run A, the gyroscope consists of a Homosil quartz rotor and a ceramic housing designed for laboratory use, and for runs B and C, the gyroscopes consist of a Homosil quartz rotor and a flight development quartz housing. The table includes columns for the mass unbalance A_c estimated from the measured niobium coating thickness, the measured precession rate in the laboratory frame, the spin speed range during the precession measurement, and the mass-unbalance component parallel to the spin axis A_p inferred from the observed precession rate assuming it is solely the result of a mass unbalance and the earth's rotation rate. The two estimates of the mass unbalance are of the same approximate magnitude, with $A_p < A_c$. This implies, although not with certainty, that the coating uniformity may be the dominant contribution to the mass unbalance.
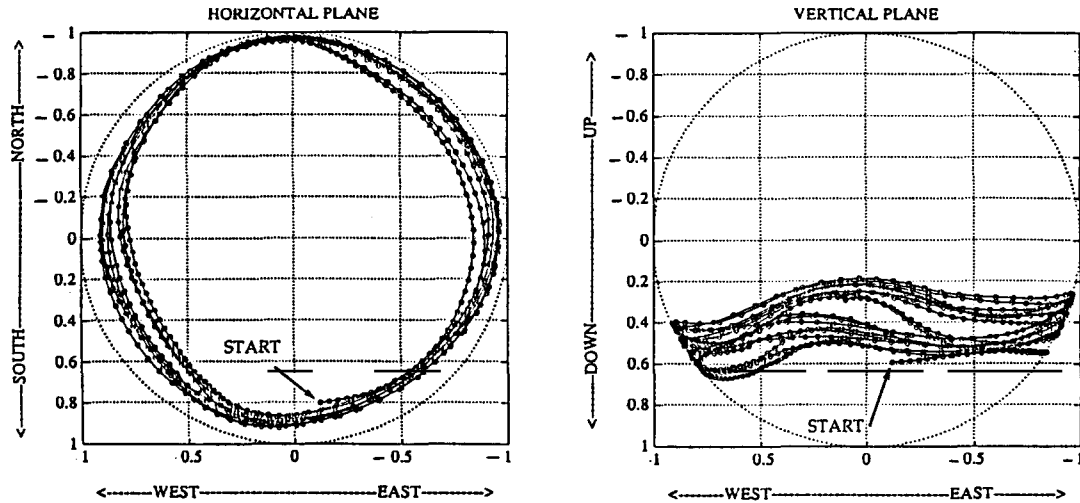
Fig. 3.   Precession of gyroscope in the laboratory frame.   Unit gyro spin vector
data are plotted as circles at intervals of 90 s.   Two projections in the labora-
tory coordinate frame are shown: one in the horizontal plane whose coordinates are
the geographical directions, and one in a vertical plane.

TABLE 2   Summary of Data for Low-Temperature Gyro Tests

Run	Rotor	Mass Unbalance* A_c (nm)	Precession Rate Laboratory Frame (°/hour)	Spin Speed (Hz)	Mass Unbalance** A_p (nm)
A	86-3H	45	43	1.53-1.21	33
B	86-4H	80	103	1.52-1.27	62
C	87-1H	30	15	18.9-14.7	23

*Estimated from the niobium coating thickness data.
**Component parallel to spin axis estimated from the precession rate.

Three general classes of Newtonian torques can disturb the gyroscope: (1) a mass-unbalance
torque that scales with the average acceleration transverse to the gyro axis, (2) electro-
static suspension torques that depend on a number of factors such as acceleration and
suspension preload, and (3) torques that depend neither on acceleration or suspension voltage
(e.g., differential gas damping).   For the mass-unbalance torque, the laboratory data can be
used to infer its contribution to the precession rate of a gyroscope under flight conditions
(3×10^{-11} g average acceleration transverse to the gyro axis and a gyro spin speed of 170 Hz);
for the gyroscope in run C, the contribution to the flight precession rate would be
0.3×10^{-3} arc-sec/yr assuming the gyroscope was spinning about the same body axis as in the
laboratory experiment.   This rate would meet the GP-B disturbance precession rate requirement
if it were the sole source of Newtonian torques.   In the future, it may be possible to set
similar limits on the other two categories of disturbance torque.   For the second category,
this means very careful modeling of precise experimental precession data, and for the last
category, possibly making very precise measurements of the gyro spin-down rate.

Low-temperature, ultrahigh vacuum bakeout.   Differential gas damping torques require that the
helium gas pressure between the rotor and the housing be less than 10^{-10} torr to keep the
disturbance precession rate from this source below 0.1×10^{-3} arc-sec/yr /3/.   After helium gas
spinup, it is difficult to remove the adsorbed helium from the gyroscope and its low-
temperature environment.   An experiment was carried out in the gimballed gyro test facility
to determine if low-temperature, ultrahigh vacuum bakeout is effective in reducing the helium
pressure in the vacuum can surrounding the gyroscope.   Without pumping, helium gas was
admitted into the gyroscope and vacuum can until it reached a pressure of about 10^{-4} torr
(similar conditions to spinup).   The vacuum region was then pumped with a turbomolecular pump
while the gyro and its low-temperature environment were heated to 7 K for 1.5 hours.   The
temperature was then reduced to 5 K and, after 0.5 hour, the pressure in the vacuum can
dropped to 4×10^{-11} torr, below the 10^{-10} torr requirement.   It remains to be shown by calcu-
lation that the pressure between the rotor and the housing will also meet this requirement.

Spinup of Gyro to High Spin Speed at Room Temperature

A niobium coated fused-quartz rotor suspended in a laboratory ceramic housing was spun up at room temperature with nitrogen gas to 177 Hz, 7 Hz above the flight baseline spin speed of 170 Hz. The spin speed was measured with an electronic stroboscope. No changes in the signals associated with the electrostatic suspension electronic system were observed, thus demonstrating that the gyroscope and its suspension system correctly function for spin speeds up to 177 Hz.
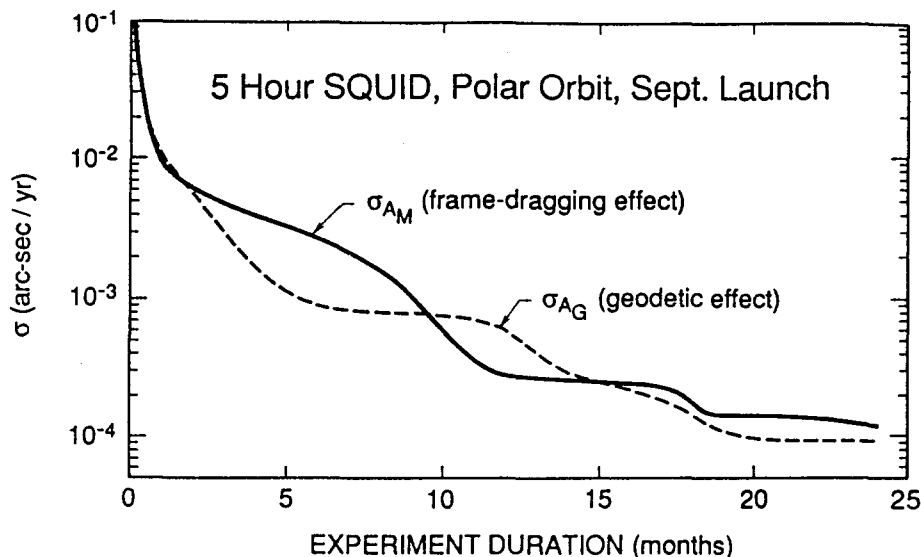

Fig. 4. Errors for the geodetic and frame-dragging effects due to noise in the experiment readout chain as a function of mission duration. The errors are estimated using a Kalman filter covariance analysis.

GYRO READOUT & MAGNETIC SHIELDING

A spinning superconducting gyro rotor produces a London magnetic moment which is aligned with the gyro spin axis. For the 38 mm diameter GP-B rotor spinning at 170 Hz, the magnitude of the magnetic moment is 2×10^{-4} G-cm^3. The gyro readout consists of a five-turn, thin-film superconducting readout loop (wound around the gyro rotor) connected to the input of a superconducting quantum interference device (SQUID). Initially, the direction of the London moment is located in the plane of the readout loop. As the angle between the gyro and the plane of the readout loop changes, magnetic flux is coupled to the readout loop resulting in a SQUID output proportional to angle. The gyro readout is referenced to the fixed stars since the readout loop is mechanically coupled to the telescope pointed at the guide star Rigel (the readout loop plane is aligned parallel to the telescope axis) and to a star blipper looking approximately normal to the telescope axis. The spacecraft together with the readout loop rolls about the line-of-sight to Rigel with a roll period of 10 minutes. The SQUID output is modulated at the 1.67 mHz roll frequency. The amplitude of the 1.67 mHz output is proportional to the angle between the gyro spin axis and the roll axis, and its phase is related to the position of the stars in the field of the star blipper. Misalignment between the roll axis and the line-of-sight to Rigel can be subtracted from the SQUID output using the two-axis telescope readout signals, finally yielding an overall gyro readout.

Noise in the SQUID is expected to be the principal error source in the gyro readout. At low Fourier frequencies, SQUIDs typically exhibit an approximate f^{-1} dependence of the spectral density of noise energy. However, since the integration time is long compared to the period of the signal frequency, the energy spectral density to first order can be taken as white in the vicinity of the signal bandwidth. This simplification allows a SQUID, when well coupled to the five-turn readout loop and when the gyro spin speed is 170 Hz, to be characterized by the integration time τ_{squid} required to reach an estimated gyro readout error of 1×10^{-3} arc-sec assuming that there are no other noise sources in the readout system. For longer measurement times, the readout error will scale as $\tau^{-0.5}$.

The standard errors for the geodetic and frame-dragging effects due to noise in the complete experiment readout chain have been estimated using a Kalman filter covariance analysis whose results are plotted in Figure 4 as a function of experiment duration for a September launch. The noise sources included in this analysis are SQUID noise with τ_{squid} = 5 hours, noise in
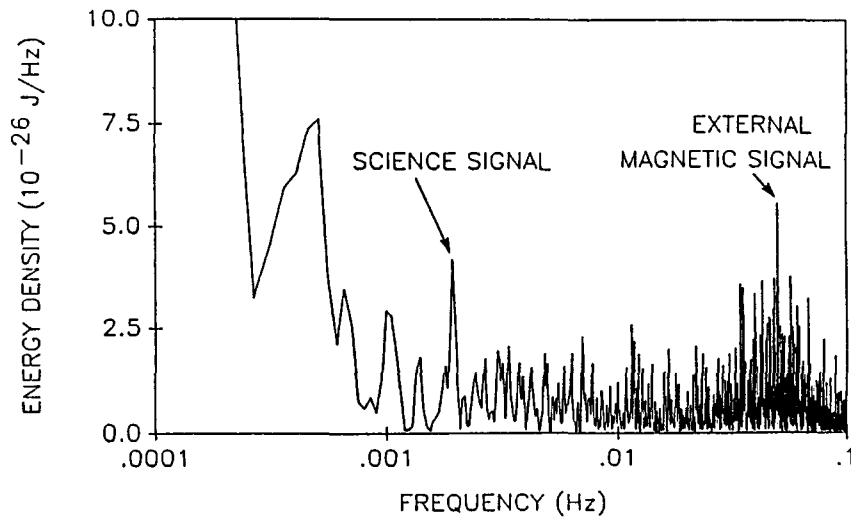
Fig. 5.   Readout-signal energy spectral density versus Fourier frequency for one
test run in Readout Test B.   Two signals are observed above the noise: a simulated
signal equivalent to 0.1 arc-sec at 1.67 mHz, and a signal due to a 2 G magnetic
field at 0.05 Hz applied to the open end of the magnetic shielding system.

the readout scale factor, and noise in the angle between the readout loop and the star
blipper.   Further, the readout scale factor and readout roll angle are determined in the
analysis using the precisely known values of the orbital and annual aberration of starlight
from Rigel.   As can be seen in Figure 4, the experiment readout-chain error requirements
given in the introduction are reached in 13 months for the geodetic effect and in 12 months
for the frame dragging effect both of which are shorter than the expected experiment duration
of at least 18 months.   If T_{squid} is assumed to be 70 hours, an earlier analysis yields the
need for a 21 month experiment duration /13/.

If the gyro readout were unshielded from the earth's magnetic field, the experiment would
contain a very large signal from this source at roll frequency.   To keep this unwanted signal
low, the gyro readout is magnetically shielded with a multi-component system consisting of
(from the outside to inside) a ferromagnetic shield, a superconducting lead bag shield, a
separate local superconducting niobium shield around each gyroscope, and the self shielding
of the superconducting gyro rotor.   This shielding system is designed to provide an ac
shielding factor of 5×10^{12} and a dc residual field of $< 10^{-7}$ G.   The low dc residual field is
needed to allow low trapped magnetic flux in the spinning rotor and thus to prevent
saturation and maintain linearity in the readout system.   The ac shielding factor of 5×10^{12}
reduces the unwanted signal from the earth's magnetic field to an equivalent angle of about
0.2×10^{-3} arc-sec.   However, since this signal is nearly constant (after orbital and daily
averaging) over the year, it should not appear as a precession rate nor contribute
significantly to the readout error.

SQUID Noise Measurements

As discussed above, the experiment readout-chain contribution to the standard errors of the
relativity effects depends strongly on SQUID noise and the parameters of the readout system.
Earlier measurements of the low-frequency noise of a commercial rf SQUID with a shorted input
imply T_{squid} of 150-200 hours /14/.   It is the goal of the GP-B experiment to have a readout
system with $T_{squid} < 5$ hours.   Efforts are underway to attain this goal through the use of
very low noise dc SQUIDs and possibly of advanced readout loop structures.   Dc SQUIDs having
very favorable shorted-input, open-loop noise levels have been reported /15,16/.   Similar
devices are currently being tested in the flux-locked loop configuration at Stanford.   Recent
low-frequency noise measurements from these tests indicate a spectral density of noise energy
at 1.67 mHz of less than 3×10^{-29} J/Hz /17/.   This noise level leads to $T_{squid} < 5$ hours
assuming that such a SQUID is well coupled to the readout loop and that no significant noise
is added by other parts of the readout system.

Readout Test B

A gyro readout and magnetic shielding system which is prototypical of flight design concepts
and whose hardware components are approximately full size is now being tested.   The testing
of this system is called Readout Test B.   The gyro readout consists of a stationary niobium-
coated quartz rotor located inside of a partially machined flight development quartz housing,
a single-turn, thin-film niobium readout loop on the readout housing half, and a commercial

rf SQUID (biased at 200 MHz) whose input is connected to the readout loop. The London-moment signal is simulated by passing a current through a second thin-film loop located around the readout loop. The gyro readout is shielded with a local superconducting niobium shield around the readout loop and gyroscope, a superconducting lead bag, and a ferromagnetic shield. The superconducting lead bag, which has a 200 mm diameter (instead of the 250 mm flight baseline), has been shown to have a residual dc field of $< 9\times10^{-8}$ G /18/.

In the first experimental run of the Readout Test B system, the niobium coated quartz rotor was not included. Figure 5 is the readout energy spectral density for data coming from one of the tests in the first experimental run. For this test, during which data were collected for 6 hours, a 0.1 arc-sec simulated signal at 1.67 mHz was magnetically coupled to the readout loop and a 2 G magnetic field at 0.05 Hz was applied to the open end of the ferromagnetic shield. (The applied field was transverse to the shield axis and to the readout loop plane.) Several important conclusions can be drawn from the experimental conditions and the spectral density shown in Figure 5. First, the 1.67 mHz simulated signal appears in the spectrum as expected, about 0.04 (in energy) times that expected for a five-turn loop. Second, the estimated spectral density of noise energy at 1.67 mHz is 8×10^{-27} J/Hz. This noise level is essentially all the result of white noise added by a shunt resistor across the SQUID input. Without this shunt, the noise would be a few $\times$ 10^{-27} J/Hz which is comparable to that reported for a similar SQUID with a shorted input (1.7×10^{-27} J/Hz) /14/. Finally, from the signal observed at 0.05 Hz, the magnetic shielding factor is estimated to be 2×10^{10}. Inclusion of the rotor shielding element in the next test will yield the first shielding factor measurement for the complete shielding system.
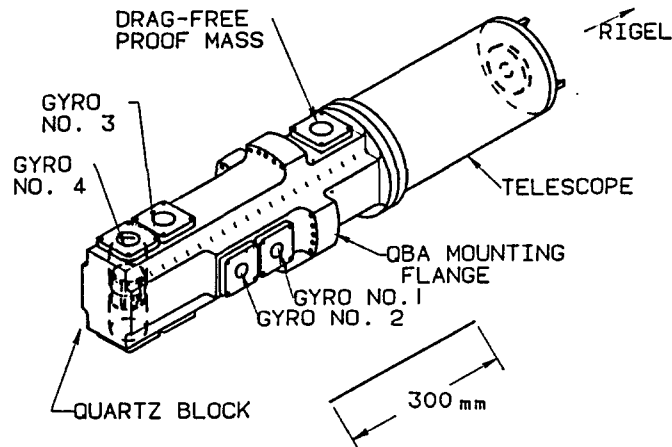

Fig. 6. Isometric view of quartz-block assembly.

FIRST INTEGRATED SYSTEM TEST

To establish experience and understanding in GP-B flight design and integration concepts, a full-size prototypical ground test instrument is now under development. The development and test of this instrument is called the First Integrated System Test (FIST). The FIST instrument comprises three major subsystems: a quartz-block assembly (QBA), a multi-gyro probe (MGP), and an engineering development dewar (EDD). The QBA is being designed and built at Stanford University and the MGP and EDD at the Research and Development Division of Lockheed Missiles and Space Company, Inc. The design requirements and solutions for these subsystems are described elsewhere /19/.

Description of FIST Instrument

Quartz-block assembly. Figure 6 is an isometric view of the quartz-block assembly (QBA). As observed in the figure, a fused-quartz block serves to mechanically couple four gyroscopes, a drag-free proof mass, and a fused-quartz telescope. The QBA is attached to the multi-gyro probe with bolts at the QBA mounting flange shown in the figure. For FIST, the QBA consists of the quartz block, two gyroscopes (no. 1 and no. 2) each surrounded with a local superconducting niobium shield, and supporting retention hardware. A photograph of the fabricated quartz block is shown in Figure 7. The QBA design is prototypical of flight design concepts and allows the other two gyroscopes, drag-free proof mass, and telescope to be installed for later tests.

Multi-gyro probe. The quartz-block assembly is mounted in the vacuum can of the multi-gyro probe (MGP). The MGP serves many functions: it provides electrical cables, spinup gas and vacuum conduction lines, and a telescope aperture between low and room temperature; it

provides a thermal conduction path from the QBA to the liquid helium cooling; and it can be inserted into the dewar while the dewar is cold and filled with liquid helium. The MGP design is largely prototypical of flight design concepts. Although the initial MGP test article is only populated with the support (electrical, etc.) needed for two gyroscopes, there is space allocated for adding all of the support needed for the other two gyroscopes, the drag-free proof mass, and the telescope.

Engineering development dewar. The multi-gyro probe is inserted into the well of the engineering development dewar (EDD). This laboratory dewar serves to provide the 2 K temperature and the two outer layers of magnetic shielding needed for the gyroscopes and QBA. The EDD design is prototypical of flight design concepts at its thermal and mechanical interfaces with the MGP. The EDD also includes a ferromagnetic shield and a superconducting lead bag, both prototypical of flight design concepts for the magnetic shielding system.

FIST Progress

The FIST instrument hardware is now in the fabrication stage. Deliveries of the QBA, MGP, and EDD are expected to be early in 1989. A class 10 clean room facility for integration of the QBA and MGP has been recently completed, and the clean room facility for housing the FIST instrument is designed. The support equipment for FIST integration and test is currently being designed and built. The integration of the FIST instrument should commence in early 1989 and testing of the integrated instrument in mid 1989.
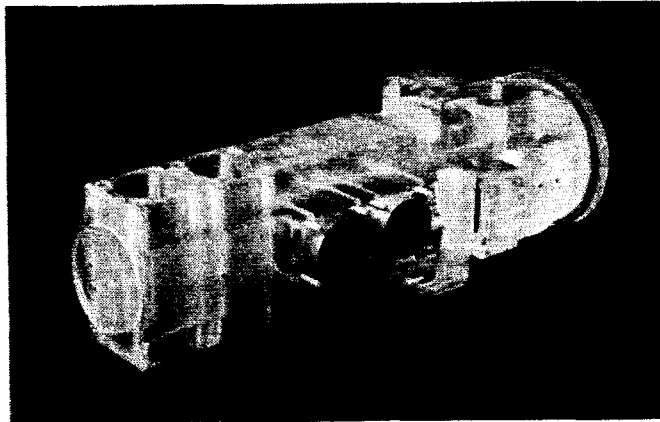

Fig. 7. Photo of quartz block after machining from a single boule of fused quartz. Niobium local magnetic shields are located in the cylindrical holes that will contain gyros no. 1 and no. 2.

CONCLUSION

Effort on the gyroscope, gyro readout and magnetic shielding system, and the development of a ground test instrument has emphasized hardware which is full size and prototypical of flight design concepts and which will support the goal of achieving measurements of the geodetic and frame-dragging effects to 0.01% and 1%, respectively. Significant progress has been made in each of these areas. Flight development gyroscopes have been designed and manufactured which are at or near the principal manufacturing requirements needed for flight. Assembled gyroscopes tested at 5 K have achieved low precession rates from which the total rotor mass-unbalance component parallel to the spin axis can be estimated. In one case the parallel component of the mass unbalance is 23 nm. Assuming such a mass unbalance were aligned along the gyro spin axis during flight conditions (3×10^{-11} g average acceleration transverse to the gyro axis and a gyro spin speed of 170 Hz), its contribution to the disturbance precession rate would be 0.3×10^{-3} arc-sec/yr. Note that 0.3×10^{-3} arc-sec/yr is the flight requirement for the disturbance rate, but of course it is the total from all sources of disturbance torque. SQUID noise measurements and the test of a nearly complete prototypical gyro readout and magnetic shielding system demonstrate significant progress toward meeting the error requirement for the experiment readout chain. Finally, the development of a full-size ground test instrument is in progress, and testing of this ground test instrument should begin in mid 1989. We expect to have the GP-B spacecraft ready for a 1995 Science Mission launch.

ACKNOWLEDGEMENTS

R. Decher, P. Peters, C. Sisk, and E. Urban of the NASA Marshall Space Flight Center; and
C. Everson and M. Mintz of the Lockheed Missiles and Space Company, Inc.

REFERENCES

1. L.I. Schiff, Motion of a gyroscope according to Einstein's theory of gravitation, Proc. Nat. Acad. Sci. 46, 871 (1960)

2. K.S. Thorne, Gravitomagnetism: Jets in Quasars, and the Stanford Gyroscope Experiment, in: Near Zero: New Frontiers of Physics, eds. J.D. Fairbank, B.S. Deaver, Jr., C.W.F. Everitt, and P.F. Michelson, W.H. Freeman, New York, 1988, p. 573

3. J.P. Turneaure, C.W.F. Everitt, B.W. Parkinson, J.T. Anderson, D. Bardas, W.S. Cheung, D.B. DeBra, W.M. Fairbank, R.A. Farnsworth, D. Gill, R. Hacker, G.M. Keiser, J.A. Lipa, J.M. Lockhart, R.A. Van Patten, R.T. Parmley, R.H. Vassar, and L.S. Young, The Gravity-Probe-B Relativity Gyroscope Experiment: Approach to a Flight Mission, in: Proc. of the Fourth Marcel Grossmann Meeting on General Relativity, ed. R. Ruffini, North-Holland, Amsterdam, 1986, p. 411

4. J.T. Anderson and C.W.F. Everitt, Limits on the measurement of proper motion and the implications for the relativity gyroscope experiment, GP-B Document No. S0020, W.W. Hansen Laboratories of Physics, Stanford University, Stanford, CA (1979)

5. T.G. Duhamel, private communication (1988)

6. R.D. Reasenberg, R.W. Babcock, J.F. Chandler, M.V. Gorenstein, J.P. Huchra, M.R. Pearlman, I.I. Shapiro, R.S. Taylor, P. Bender, A. Buffington, B. Carney, J.A. Hughes, K.J. Johnston, B.F. Jones, and L.E. Matson, Microarcsecond optical astrometry: an instrument and its astrophysical applications, Astron. J. 96, 1731 (1988)

7. G. Dunbar, Measurement of optical homogeneity of fused silica, M.Sc. Thesis, University of Aberdeen, Aberdeen, Scotland, U.K. (1981)

8. M.A. Player and G. Edgar, private communication (1988)

9. W. Angele, Finishing high precision quartz balls, Prec. Eng. 2, 119 (1980)

10. D.G. Chetwynd and G.J. Siddall, Improving the accuracy of roundness measurement, Phys. E: Sci. Instrum. 9, 537 (1976)

11. J.A. Lipa, private communication (1982)

12. P. Peters, private communication (1984)

13. R. Vassar, Error analysis for the Stanford Relativity Gyroscope Experiment, Ph.D. Dissertation, Stanford University, Stanford, CA, U.S.A. (1982); R. Vassar, J.V. Breakwell, C.W.F. Everitt, and R.A. Van Patten, Orbit selection for the Stanford Relativity Gyroscope Experiment, J. of Spacecraft and Rockets 19, 66 (1982)

14. J.M. Lockhart and J.J. Kingston, Effect of trapped flux and temperature variations on 1/f noise in rf SQUIDs, Japanese Journal of Applied Physics 26-3, 1561 (1987)

15. C.D. Tesche, K.H. Brown, A.C. Callegari, M.M. Chen, J.H. Greiner, H.C. Jones, M.B. Ketchen, K.K. Kim, A.W. Kleinsasser, H.A. Notary, G. Proto, R.H. Wang, and T. Yogi, Practical dc SQUIDs with extremely low 1/f noise, IEEE Trans. Mag. Mag-21, 1032 (1985)

16. M.W. Cromar, private communication (1988)

17. Y. Miki, B. Muhlfelder, J.M. Lockhart, C.D. Tesche, and M.W. Cromar, private communication (1988)

18. J.M. Lockhart, SQUID readout and ultra-low magnetic fields for Gravity Probe-B, in: SPIE Vol. 619 Cryogenic Optical Systems and Instruments II, SPIE, Bellingham, WA, 1986, p. 148

19. B.W. Parkinson, C.W.F. Everitt, J.P. Turneaure, and R.T. Parmley, The prototype design of the Stanford Relativity Gyro Experiment, in: Proc. of the 38th Congress of the International Astronautical Federation IAF-87-458, American Institute of Aeronautics and Astronautics, Washington, DC, 1987